Received: 9 January 2023 | Accepted: 17 April 2023

DOI: 10.1111/srt.13337

ORIGINAL ARTICLE

WILEY

Autophagy gene Atg7 regulates the development of radiation-induced skin injury and fibrosis of skin

Xinyi Chen | Wan Qin | Lu Wang | Yu Jin | Jingyao Tu | Xianglin Yuan

Department of Oncology, Tongji Hospital, Tongji Medical College, Huazhong University of Science and Technology, Wuhan, Hubei, China

Correspondence
Xianglin Yuan, Department of Oncology, Tongji Hospital, Tongji Medical College, Huazhong University of Science and Technology, Jie Fang Rd 1095, Wuhan, Hubei Province, China.Wuhan, China.
Email: yuanxianglin@hust.edu.cn

Funding information
National Natural Science Foundation of China, Grant/Award Number: 82130092

Abstract

Background: Radiation-induced skin injury, which may progress to fibrosis, is a severe side effect of radiotherapy in patients with cancer. However, currently, there is a lack of preventive or curative treatments for this injury. Meanwhile, the mechanisms underlying this injury remain poorly understood. Here, we elucidated whether autophagy is essential for the development of radiation-induced skin injury and the potential molecular pathways and mechanisms involved.

Methods and results: We used the myofibroblast-specific Atg7 knockout (namely, conditional Atg7 knockout) mice irradiated with a single electron beam irradiation dose of 30 Gy. Vaseline-based 0.2% rapamycin ointment was topically applied once daily from the day of irradiation for 30 days. On day 30 post irradiation, skin tissues were harvested for further analysis. In vitro, human foreskin fibroblast cells were treated with rapamycin (100 nM) for 24 h and pretreated with 3-MA (5 mM) for 12 h. Macroscopic skin manifestations, histological changes, and fibrosis markers at the mRNA and protein expression levels were measured. Post irradiation, the myofibroblast-specific autophagy-deficient ($Atg7^{Flox/Flox}$ Cre^{+}) mice had increased fibrosis marker (COL1A1, CTGF, TGF-β1, and α-SMA) levels in the irradiated area and had more severe macroscopic skin manifestations than the control group ($Atg7^{Flox/Flox}$ Cre^{-}) mice. Treatment with an autophagy agonist rapamycin attenuated macroscopic skin injury scores and skin fibrosis marker levels with decreased epidermal thickness and dermal collagen deposition in $Atg7^{Flox/Flox}$ Cre^{+} mice compared with the vehicle control. Moreover, in vitro experiment results were consistent with the in vivo results. Together with studies at the molecular level, we found that these changes involved the Akt/mTOR pathway. In addition, this phenomenon might also relate to Nrf2-autophagy signaling pathway under oxidative stress conditions.

Conclusion: In conclusion, Atg7 and autophagy-related mechanisms confer radioprotection, and reactivation of the autophagy process can be a novel therapeutic strategy to reduce and prevent the occurrence of radiodermatitis, particularly skin fibrosis, in patients with cancer.

KEYWORDS
autophagy, fibrosis, oxidative stress, radiodermatitis, rapamycin

1 | INTRODUCTION

Radiation therapy is normally used to treat several types of cancers.[1] However, the major side effect of radiation therapy is cutaneous tissue injury, also called radiodermatitis, which occurs in 95% of patients with cancer receiving radiation therapy.[2,3] In fact, after any form of radiotherapy, the skin will be inevitably affected to varying degrees. The early visible sign of cutaneous reaction is erythema, which occurs in 90% of patients, and this type of symptom can evolve into desquamation or even into ulcers at an advanced stage.[4] Up to 25% of patients develop severe skin reactions, leading to necrosis and scarring. Unfortunately, patients with these complications tend to interrupt radiation treatment planning, which may increase the risk of cancer recurrence.[5] In advanced stages, skin/muscle fibrosis caused by radiation is one of the most significant late side effects of radiation exposure, characterized by an abnormal wound healing response, leading to excessive deposition of extracellular matrix (ECM) at the site of radiation injury.[6,7] Furthermore, various studies have attempted to determine effective interventions against skin injuries caused by radiation exposure, such as washing, dermatitis agents (hyaluronic acid, corticosteroid, sucralfate cream), antioxidant agents (vitamin C and vitamin E), and wound dressing (hydrogel)[8]; however, the therapeutic effects of conservative treatment are unsatisfactory. Therefore, further investigation is required to determine the underlying mechanism of radiation-induced skin injury to guide the development of novel therapeutic strategies.

Macroautophagy (hereafter referred to as autophagy) is a well-conserved cellular degradative pathway in cells, along with the ubiquitin–proteasome system. In autophagy, intracellular components are sequestered by autophagosomes and then fused with lysosomes to degrade and recycle the sequestered substrates.[9] Several lines of evidence have suggested that autophagy may serve as a protective mechanism against the progression of several human diseases, including cancer, muscular disorders, and neurodegeneration.[10] Studies have also shown that autophagy regulates ultraviolet radiation-induced inflammation and skin tumorigenesis.[11] More recently, a study by Qiang et al. demonstrated that keratinocyte autophagy deficiency reduces stem cell self-renewal capability and regenerative potential, eventually resulting in difficult-to-heal cutaneous wounds.[12] In addition, as indicated in the study by Hao et al., autophagy activation appears to be a cytoprotective process in response to UVB-induced skin photodamage.[13] It is well known that radiation-induced injury can involve various tissues and organs. Given that our research group has a long-standing commitment to the search for occurrence and prevention of side effects related to radiotherapy, and some achievements have been made in the relevant field,[14–18] there is great interest in side effects of radiotherapy. However, the association between autophagy and radiation-induced skin injury has not yet been determined. It seems to be a research direction worth further exploration.

Given that Atg7-deficient mice died within postnatal day 1,[19] we considered using the conditional Atg7 knockout model for the current study. Myofibroblasts, as the major source of excessive ECM synthesis under the pathophysiological conditions that characterize fibrosis, are the critical effector cells in the pathological process of radiation fibrosis.[20,21] Therefore, we decided to conditionally knock out Atg7 in myofibroblasts. In this way, the potential effect of autophagy on the process of radiation fibrosis can be evaluated in a more convincing way. Herein, to determine the roles of autophagy in radiation-induced injury, Atg7 conditional knockout mice were generated using the Cre-LoxP method.[19] Using mice with a myofibroblast-specific Atg7 deletion, we demonstrate an unexpected consequence of autophagy deficiency in the progression of radiation-induced skin injury and fibrotic changes through the Akt–mTOR pathway. In addition to classical autophagy pathways, autophagy deficiency resulted in aberrant nuclear factor E2-related factor 2 (Nrf2) pathway activation in response to oxidative stress. Importantly, the induction of autophagy by rapamycin effectively attenuates these symptoms. Our findings potentially provide a mechanistic association among autophagy, radiation-induced skin injury, and fibrotic changes following radiation therapy. These findings suggest a potential therapeutic strategy to reduce and prevent the occurrence of radiodermatitis, particularly skin fibrosis in patients.

2 | MATERIALS AND METHODS

2.1 | Cell cultures and irradiation

Human foreskin fibroblast (HFF-1) cells (obtained at passage 4) were purchased from Zhong Qiao Xin Zhou Biotechnology (Catalog No. ZQ0450; https://www.zqxzbio.com/Index/p_more/pid/861.html; Shanghai, China). Cells were maintained in DMEM supplemented with 10% fetal bovine serum (Gibco, USA) and 1% penicillin/streptomycin at 37°C in a humidified atmosphere with 5% CO_2. Two days (48 h) after siRNA transfection, cells were irradiated with a single dose of 8 Gy using a clinical linear accelerator (6Mv x-rays, Elekta Precise, Stockholm, Sweden). Autophagy inhibitor 3-methyladenine (3-MA) was purchased from MCE (HY-19312), pretreating HFF-1 cells with 5 mM for 12 h before irradiation. After irradiation, cells were treated with rapamycin (MCE, AY-22989, 100 nM) for 24 h.

2.2 | Generation of Atg7 conditional knockout mice

The $Atg7^{Flox/Flox}$ mouse BRC No. RBRC02759,[19,22] with a strain name of B6; Cg-$Atg7^{tm1Tchi}$, was purchased from the Model Animal Research Center (Nanjing, China; stock number D000534). Pdgfrb-Cre^{+} mice, named as Tg(Pdgfrb-cre)^{35Vli}, were a generous gift from Dr.

Volkhard Lindner[23] (Center for Molecular Medicine, Maine Medical Center Research Institute, USA). Atg7$^{Flox/Flox}$ (Atg7$^{F/F}$) mice, carrying floxed alleles for the autophagy gene Atg7, were crossed with Pdgfrb-Cre mice to obtain Atg7$^{Flox/Flox}$ Pdgfrb-Cre^{-} (Control) and Atg7$^{Flox/Flox}$ Pdgfrb-Cre^{+} (Atg7 conditional knockout) mice, resulting in myofibroblast-specific autophagy deficient. The genotypes of these mice were determined by PCR analysis. Approximately 6–8-week-old mice were used for the experiments. The animals were kept under standard laboratory conditions, and the Tongji Hospital Institutional Review Board of Experimental Animals approved all of the experimental protocols.

2.3 | Genotyping

DNA extraction was performed according to the protocol of the One Step Mouse Genotyping Kit (Vazyme Biotech, Nanjing, China) using mouse tails. DNA extracts (2 μL) were added to a 20 μL PCR reaction system containing 2× Taq Plus Master Mix, primers and nuclease-free water (Vazyme Biotech, Nanjing, China). The PCR conditions were as follows: initial denaturation at 95°C for 3 min, then 30 cycles at 95°C for 15 s, 60°C for 15 s, and 72°C for 1 min, with final extension at 72°C for 5 min. DNA amplification was conducted in a S1000 Thermal Cycler (Bio-Rad, USA). Amplified fragments were separated on a 2% agarose gel containing SuperRed/GelRed (Biosharp, Wuhan, China) under standard electrophoresis conditions and visualized under a UV light illuminator. Genotype was analyzed using primers and PCR conditions described previously.[19,22,24,25] The primers used in the PCR were as follows: Flox forward primer: 5′-TGGCTGCTACTTCTGCAATGATGT-3′, reverse primer: 5′-GAGGACAGAGACCATCAGCTCCAC-3′; ATG7 wild-type (WT) forward primer: 5′-ATTGTGGCTCCTGCCCCAGT-3′, reverse primer: 5′-GAGGACAGAGACCATCAGCTCCAC-3′; Cre forward primer: 5′-GCATTTCTGGGGATTGCTTA-3′, reverse primer: 5′-CCCGGCAAAACAGGTAGTTA-3′.

2.4 | Mouse model of radiation-induced skin injury

We conducted a 30-day study using 6–8-week-old male and female Atg7$^{Flox/Flox}$ Pdgfrb-Cre^{-} (Atg7$^{F/F}$ Cre^{-}, as the control group) or Atg7$^{Flox/Flox}$ Pdgfrb-Cre^{+} (Atg7$^{F/F}$ Cre^{+}, as the experimental group) mice ($n \geq 3$ per group). Mice were shaved using an electric razor in the dorsal areas, and anesthetized with 1.5% pentobarbitone (50 mg/kg, i.p.). Anesthetized mice were placed prone with a 2 cm square lead cut-out to direct the beam onto the mouse dorsal areas. Dermatitis was induced in each group by exposing the animals' dorsal areas to a 30 Gy dose electron beam. To increase the skin dose to a maximum, 1.0 cm-thick build-up material was placed on the dorsal areas of each mouse. All of experimental groups received irradiation. The number of animals per group selected for these experiments (n = 6) was based upon the power calculation formula as previously reported by Arifin and Zahiruddin.[26] All of the animals used in the study were housed in the Animal Center of Tongji Hospital, Tongji Medical College, Huazhong University of Science and Technology (HUST, Wuhan, China).

2.5 | Topical medications

Bulk rapamycin powder purchased from MCE (Shanghai, China; AY-22989) was mixed with vaseline to constitute the vaseline-based 0.2% rapamycin ointment. The rapamycin ointment was then divided into aliquots and stored at −80°C until application. We selected rapamycin ointment with 0.2% concentration in the present study as per the previous study.[27]

2.6 | Assessment for Masson's trichrome staining images

On day 30, mice were sacrificed by cervical dislocation, and the dorsal skins were fixed in 4% paraformaldehyde and embedded in paraffin. The tissue sections were stained with Masson's trichrome reagent to evaluate morphological changes, particularly including collagen deposits and epidermal thickness. Images of the trichrome-stained area were captured using CaseViewer software at 100× and 400× original magnification. Epidermal thickness was quantified in the Masson-stained sections by using ImageJ. For each image, epidermal thickness was determined by taking the average of 10 equally spaced points along the length of the tissue in a blinded manner. To measure the collagen density in the skin, the areas of the collagen fibers and the entire section were measured by counting the pixels in the images. Using ImageJ software, thresholding was used to select only blue pixels (collagen) so that the region of interest (ROI) (the dermis) was selected and only the area containing collagen was included in the analysis. The collagen density was calculated as the number of pixels representing collagen divided by the total number of pixels in the ROI.

2.7 | Immunohistochemical examinations

Immunohistochemical staining was performed to assess the expression of α-smooth muscle actin (α-SMA) and vimentin. In brief, the paraffin-embedded dorsal skin sections were deparaffinized, rehydrated, and subjected to antigen retrieval. Next, the samples were incubated for 30 min at room temperature in 5% bovine serum albumin, and then incubated with a 1:200 dilution of monoclonal mouse anti-α-SMA (BM0002; Boster, China) or a 1:1000 dilution of polyclonal rabbit anti-vimentin (10366-1-AP; Proteintech, China) overnight at 4°C. The sections were then washed with Tris Buffered Saline with Tween-20 (TBST), incubated with HRP-conjugated goat anti-mouse (1:5000) for 60 min at room temperature, and with 3,3′-diaminobenzidine (DAB) as a substrate. Then sections were washed with TBST three times for 5 min each. Finally, the sections were counterstained with hematoxylin, and mounted. Immune-positive cells were measured with the ImageJ software.

2.8 | Immunofluorescence examinations

Paraffin-embedded skin sections were deparaffinized and then rehydrated through descending ethanol concentrations for 5 min each, and rinsed in double-distilled water. The antigens were retrieved in citrate buffer pH 6.0 in autoclave for 2 min and cooled to room temperature. After three washes with TBS, sections then were incubated with blocking buffer (10% normal donkey serum) at room temperature for 20 min. Sections were incubated with LC3B (18725-1-AP, Proteintech), ATG7 (A0691, ABclonal), and PDGFRB (A2180, ABclonal) at 1:200 in 2% BSA in PBST at 4°C overnight, followed by Alexa Fluor secondary antibody-conjugated fluorophores (Alexa Fluor594 donkey anti-rabbit, A21206, Life Technologies) incubated at 37°C for 30 min (protect from light). Sections were mounted in Prolong Gold Antifade Reagent containing DAPI (Roche 216276), and images were captured with CaseViewer.

2.9 | Evaluation of radiation-induced skin injury

Radiation-induced skin reactions were assessed according to the Radiation Therapy Oncology Group (RTOG) criteria[7] as follows:

1. Normal;
2. Erythema;
3. Dry desquamation;
4. Moist desquamation;
5. Ulceration, hemorrhage, and necrosis.

2.10 | Real-time RT-PCR

Skin tissue of mice for RT-PCR analysis was collected in TRIzol (Takara, Japan). The RNA concentration was measured by NanoDrop 2000 (ThermoFisher Scientific). cDNA synthesis was performed using a S1000 Thermal Cycler (Bio-Rad, USA) following the manufacturer's instructions. qPCR was performed by a 7900HT Fast Real-Time PCR System (ThermoFisher Scientific) with 2× SYBR Green qPCR Master Mix (low ROX) kit (Bimake, China). The qPCR thermal cycling conditions were as follows: initiation at 95°C for 10 min for hot start, followed by 40 cycles at 95°C for 15 s and 60°C for 1 min. All primers for mouse (Atg7, Becn1, Map1lc3b, Col1a1, Ctgf, Tgfb1, Acta2, Nrf2, Nqo1, Ho-1, and Actb) and human (ATG7, COL1A1, CTGF, TGFB1, ACTA2, NRF2, NQO1, HO-1, and ACTB) were synthesized by TSINGKE (Beijing, China). All the primer sequences are listed in Table S1.

2.11 | Western blot analysis

Total proteins from mice skin tissues were extracted using RIPA buffer containing 1% PMSF. The total protein was determined by BCA protein assay kits (BOSTER, Wuhan, China) following the manufacturer's protocol. Afterward, the proteins were separated by electrophoresis (concentration gel voltage 70 V, separation gel voltage 100 V, electrophoresis time 120 min). Following electrophoresis, the separated proteins were transferred onto a polyvinylidene fluoride (PVDF) membrane by wet transfer method (at a current of 200 mA, transfer time 120 min, supplemented with 20% methanol). The membranes were blocked by incubation with 5% non-fat skim milk in TBS-T buffer, followed by incubation with antibody anti-COL1A1 (1:1000; 72026; CST), anti-TGF-β (1:1000; 3709; CST), anti-CTGF (1:1000; 86641; CST), anti-SQSTM1/p62 (1:1000; 23214; CST), anti-LC3B (1:1000; 3868; CST), anti-mTOR (1:1000; 2983; CST), anti-P-mTOR (1:1000; 5536; CST), anti-Akt (1:1000; 4691; CST), anti-P-Akt (Ser473) (1:1000; 4060; CST), anti-α-SMA (1:1000; BM0002; Boster), anti-KEAP1 (1:500; A1820; ABclonal), anti-NQO1 (1:1000; A19586; ABclonal), anti-NRF2 (1:1000; 12721; CST), anti-HO-1 (1:1000; 43966; CST), or anti-GAPDH (1:5000, AC002, Abclonal) at 4°C overnight. The membranes were washed in TBST and incubated with a corresponding secondary antibody (HRP-conjugated goat anti-rabbit IgG or goat anti-mouse antibody, 1:10 000) for 1 h at room temperature. The proteins were visualized with an enhanced chemiluminescence (ECL) kit (Thermo Fisher Scientific) using the G:BOX Chemi X system (Syngene).

TABLE 1 List of the siRNA sequences.

Gene	Sequences
si-ATG7-1	5′-GAACGAGTATCGGCTGGAT-3′
si-ATG7-2	5′-GATGTCGTCTTCCTATTGA-3′
si-ATG7-3	5′-ACTCGAGTCTTTCAAGACT-3′
si-NC	5′-TTCTCCGAACGTGTCACGTdTdT-3′

2.12 | Transfection of cells with ATG7 siRNA

Small interfering RNAs (siRNAs) targeting ATG7 were obtained from RiboBio (stB0005319; Guangzhou, China). Transfection of siRNA oligonucleotides was performed using Ribo FECT CP transfection kit (RiboBio, Guangzhou, China) according to the manufacturer's instructions. Non-targeted control siRNA (siNC) was used as negative control, and siNC was also obtained from RiboBio (Guangzhou, China). After transfection, the cells were incubated for 24–48 h and were used as required. The sequences of siRNAs are listed in Table 1.

2.13 | Lentiviral transduction for autophagy flux analysis

Adenovirus expressing mCherry-GFP-LC3B fusion protein was purchased from OBIO Technology Corp., Ltd (H6687, Shanghai, China) and used to monitor autophagy status. Cells were seeded into six-well plates and allowed to reach ~50% confluence at the time of Ad-mCherry-GFP-LC3B transfection. Lentivirus transfection was performed according to the manufacturer's instruction. Fluorescence images were captured using florescence inverted microscope (DMI3000B, Leica, Germany). The mCherry-GFP-LC3B was present

in the cytoplasm, and the autophagic flux was measured by counting the yellow ($GFP^+mCherry^+$) and red puncta ($GFP^-mCherry^+$), which indicate the presence of autophagosomes and autolysosomes, respectively.

2.14 | Protein interaction network construction

The GeneMANIA (http://genemania.org/) and STRING (https://cn.string-db.org/) databases were used to screen the proteins interacting with Atg7.

2.15 | Statistical analysis

Statistical analyses were performed using GraphPad Prism 8 software (GraphPad Software Inc., San Diego, CA, USA). The bars in the results indicate the mean values ± standard error of the mean (SEM). A two-tailed, unpaired Student's *t*-test was used to compare two groups unless otherwise stated. Lesion severity was analyzed by the Mann–Whitney *U* test. Results were considered significantly different when $p < 0.05$.

3 | RESULTS

3.1 | Murine model of radiation dermatitis

Given that Atg7-deficient mice died within postnatal day 1,[19] we generated a myofibroblast-specific Atg7 knockout mouse by crossing $Atg7^{Flox/Flox}$ mice with transgenic mice expressing Cre recombinase under the control of the Pdgfrb promoter (Pdgfrb-Cre). In Pdgfrb-Cre mice, Cre is known to be selectively expressed in myofibroblast in the dermis,[23] and this allowed us to achieve myofibroblast-directed Atg7 knockout (hereafter called $Atg7^{Flox/Flox}$ Pdgfrb-Cre) using the Cre/loxP system.

Several studies on radiation-induced skin injury in mice irradiated the dorsal skin with x-rays[28] or γ radiation.[29] Given the depth of penetration of γ rays, the injury in this model might not be limited to the skin but also extends to deeper tissues and organs. We used a model in which the skin was more selectively exposed to radiation. The strength of the electron beam is that it has a limited penetration depth and is commonly used in human radiotherapy. There has also been some evidence demonstrating that the electron beam can be used to construct a radiation-induced skin injury model in mice.[30] To this end, the dorsal skin of mice was shaved, and the dorsal areas were exposed to an electron beam from a linear accelerator (Elekta Synergy, Elekta, Stockholm, Sweden). To limit the field of exposure, except for the irradiation field (dorsal skin, 2 × 2 cm), all parts of the body were protected by a lead plate. To limit the depth of penetration, a 1.0-cm tissue equivalent material was placed between the skin and radiation source (Figure 1A).

To explore the appropriate experimental conditions, the identified wild-type (WT) mice (genotyping results of mice are shown in Figure S1) were used in the pre-experiment with an electron beam at a single dose of 15 and 30 Gy. Mice that received 15 Gy developed only mild skin injury, whereas those exposed to 30 Gy showed a significant macroscopic change. The mice irradiated with 30 Gy developed obvious macroscopic skin damage 10–20 days after irradiation compared to those exposed to 15 Gy (Figure 1B). Using the scoring system as described in the Materials and Methods section, we determined single-fraction doses of 30 Gy for subsequent experiments based on these results (Figure 1C). Meanwhile, to enhance the credibility of the myofibroblast-specific knockdown of Atg7, we performed double-immunofluorescence staining experiments with anti-Atg7/Pdgfrb on mouse skin tissues, which further confirmed the specificity of knockdown. The results revealed that Atg7 was largely suppressed in the conditional Atg7 knockout ($Atg7^{F/F}$ Cre^+) mice compared with the control group ($Atg7^{F/F}$ Cre^-) mice (Figure 1D).

3.2 | Myofibroblast-specific deletion of Atg7 in mice increased the macroscopic severity of radiation-induced skin injury

The dorsal skin of $Atg7^{Flox/Flox}$ $Cre^-$and $Atg7^{Flox/Flox}$ Cre^+ mice was exposed to a single electron beam irradiation dose of 30 Gy, and Figure 2A,B demonstrates the representative macroscopic images of the dorsal skin of mice after irradiation on different days. We found that $Atg7^{Flox/Flox}$ Cre^+ mice began to develop abnormal clinical signs of radiodermatitis at the same time as observed in $Atg7^{Flox/Flox}$ Cre^- mice, and the initial progression of the disease did not differ between the two groups (Figure 2A,B, leftmost column). Approximately 20 days after irradiation, all $Atg7^{Flox/Flox}$ Cre^+ mice developed symptoms of dry and moist desquamation, and these skin lesions further progressed into ulcers between days 20 and 30 (Figure 2B, middle and rightmost columns). Instead, most $Atg7^{Flox/Flox}$ Cre^- mice presented a relatively mild degree of skin injury at days 20 and 30 time points after irradiation and did not progress to more severe symptoms after day 20 (Figure 2A, middle and rightmost columns). Based on the scoring system described in the Materials and Methods section, we semi-quantitatively confirmed that $Atg7^{Flox/Flox}$ Cre^- mice had significantly less severe skin lesions than $Atg7^{Flox/Flox}$ Cre^+ mice 30 days post irradiation (Figure 2C). Then the expression of autophagy-related proteins p62/SQSTM1 (p62), LC3B, and Atg7 in skin tissues was detected by Western blotting. p62, A substrate for selective autophagy and degraded by autophagy, was found to be significantly increased (Figure 2D); therefore, increased p62 levels reflect impaired autophagy.[31] In summary, these results suggest that the development of radiation-induced skin injury is strongly related to autophagy levels in skin tissues.

3.3 | Myofibroblast-specific deletion of Atg7 in mice results in more pronounced skin fibrotic changes

At days 30 post irradiation, skin tissues were harvested for Masson's trichrome staining (Figure 3A). Subsequently, semi-quantification

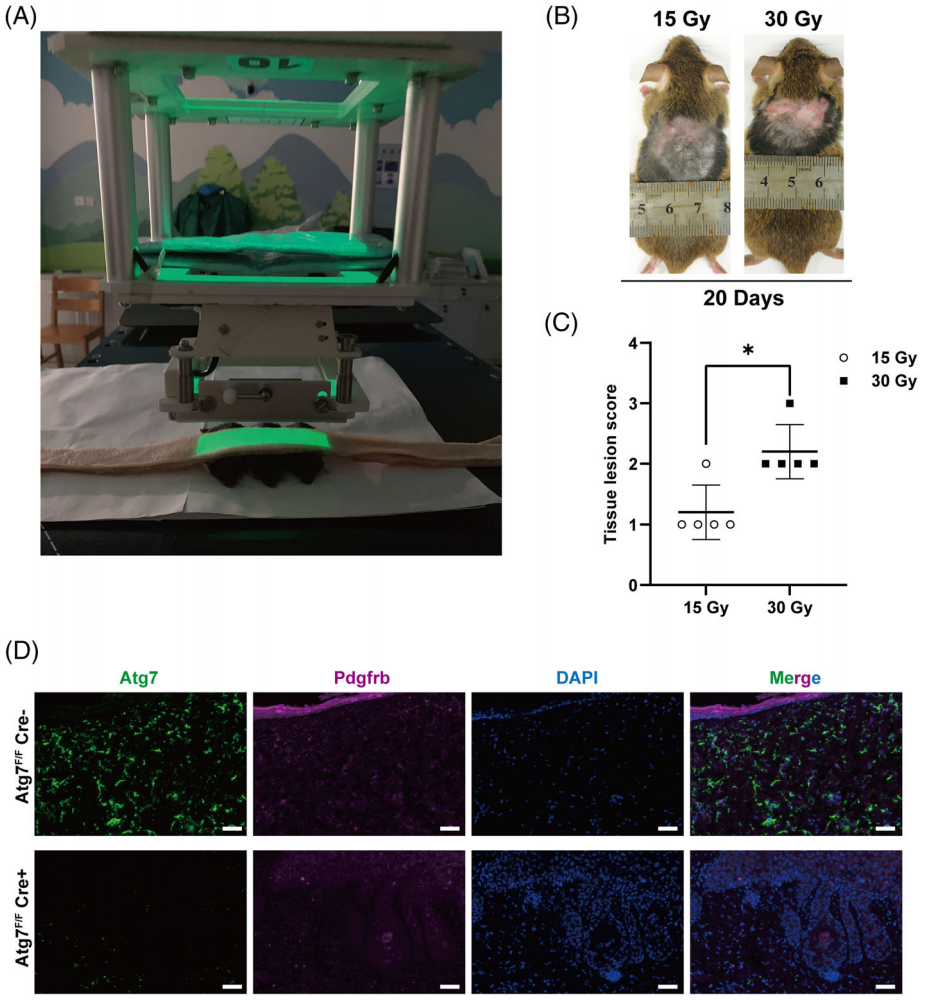

FIGURE 1 Experimental design. (A) A single fraction of 15 Gy/30 Gy with 6-MeV electrons is delivered to the dorsal skin using a linear accelerator. All parts of the body, except the irradiation field (back skin 2 × 2 cm), are protected with a lead plate, and a 1.0-cm tissue equivalent material is placed. (B) Representative photograph of the skin damage 20 days after radiation exposure. (C) RTOG score of radiation-induced dermatitis in the dorsal skin of two different groups of mice (adapted from[72]); $n = 4–5$ mice per group. (D) Immunofluorescence staining of Pdgfrb and Atg7 in the control group ($Atg7^{F/F}$ Cre^{-}) mice and myofibroblast-specific conditional Atg7 knockout ($Atg7^{F/F}$ Cre^{+}) mice. Scale bar: 50 μm. Statistical significance was estimated using the Mann–Whitney *U* test; $^{*}p < 0.05$, $Z = -2.425$.

was performed. We analyzed the epidermal thickness in Masson's trichrome staining images and observed an evident upward trend in irradiated $Atg7^{Flox/Flox}$ Cre^{+} mice compared to irradiated $Atg7^{Flox/Flox}$ Cre^{-} mice (Figure 3B). We also observed significantly higher levels of collagen deposition in irradiated $Atg7^{Flox/Flox}$ Cre^{+} mice than in irradiated $Atg7^{Flox/Flox}$ Cre^{-} mice in Masson's trichrome staining images (Figure 3C). Immunohistochemical analysis showed that the percentage of α-SMA- and vimentin-positive areas in irradiated $Atg7^{Flox/Flox}$ Cre^{+} mice was higher than that in irradiated $Atg7^{Flox/Flox}$ Cre^{-} mice group, indicating more severe fibrotic changes in the $Atg7^{Flox/Flox}$ Cre^{+} mice group than in the $Atg7^{Flox/Flox}$ Cre^{-} mice group (Figure 3D,E). In line with the histological results, the expression of several profibrotic genes, including connective tissue growth factor (CTGF), transforming growth factor β1 (TGF-β1), and α-SMA, were increased (Figure 3F). Additionally, the expression of collagen type I alpha 1 chain (COL1A1) tended to increase, but this was not statistically significant (Figure 3F). Meanwhile, the Western blot results showed an obviously increased expression of profibrotic protein, the trend of which was consistent with the RT-qPCR results (Figure 3G). Meanwhile, the autophagy-related indicators detected by immunofluorescence and qPCR analyses indicated that the autophagy flux was indeed impaired in the $Atg7^{Flox/Flox}$ Cre^{+} conditional knockout mice group (Figure 3H,I). Taken together, these data indicate that myofibroblast-specific deletion of Atg7 in mice results in more severe fibrotic changes in the skin.

3.4 | Topical rapamycin application ameliorates macroscopic severity of radiation-induced skin injury and reduces skin fibrotic changes

We then evaluated the efficacy of topical rapamycin application against radiation-induced skin injury and fibrotic changes. Rapamycin, an

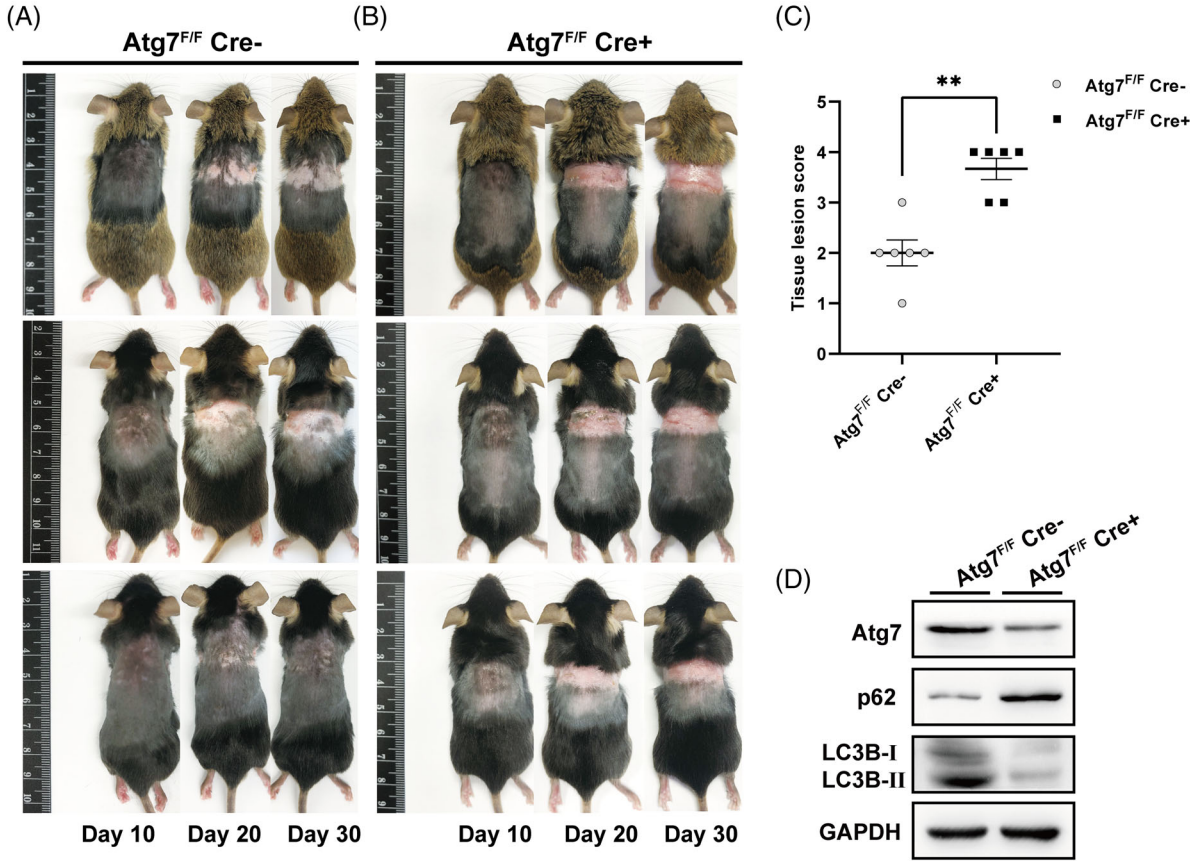

FIGURE 2 Deletion of Atg7 is a key factor for the development of radiation-induced skin injury. (A and B) Representative photographs of the dorsal skin of the two different groups ($Atg7^{Flox/Flox}$ Cre^{+} and $Atg7^{Flox/Flox}$ Cre^{-}) at different time points after irradiation. (C) RTOG score of radiation-induced dermatitis in the dorsal skin of two different groups of mice (adapted from[72]); $n = 6$ mice per group. (D) Total skin lysates of two different groups ($Atg7^{Flox/Flox}$ Cre^{+} and $Atg7^{Flox/Flox}$ Cre^{-}) at 30 days post irradiation are subjected to Western blotting analysis for p62, LC3B, and Atg7. Statistical significance was estimated using the Mann–Whitney *U* test; $^{**}p < 0.01$, $Z = -2.844$.

inhibitor of mTORC1, induces autophagy.[32] Rapamycin has previously been demonstrated to be effective against fibrosis in a systemic sclerosis (SSc) mice model[33] and has also shown potential as an antiangiogenic agent.[34] Furthermore, rapamycin has been shown to inhibit hematopoietic stem cell (HSC) proliferation and attenuates hepatic fibrosis.[35] Thus, we used rapamycin dissolved at 0.2% concentration in vaseline (the concentration was selected as previously recommended[27]), and topically applied it once daily from the day of irradiation for 30 days. Vaseline was applied topically in parallel with the vehicle control. Representative macroscopic images of irradiated skin from vehicle and rapamycin treatment groups on days 10, 20, and 30 post irradiation are shown in Figure 4A. Macroscopically, the topical application of rapamycin remarkably ameliorated the skin lesions in a time-dependent manner, leading to a significant reduction in the microscopic scoring of radiation-induced skin injury (Figure 4B). Masson's trichrome staining indicated that topical rapamycin administration significantly reduced the epidermal thickness and collagen deposition on day 30 compared to vehicle (Figure 4C,D). Additionally, immunohistochemical staining for α-SMA showed that rapamycin markedly reduced the α-SMA- and vimentin-positive areas (Figure 4E,F). These histological results indicated a substantial inhibition of fibrotic changes upon topical rapamycin treatment. Rapamycin administration also markedly decreased the mRNA levels of COL1A1, CTGF, TGF-β1, and α-SMA (Figure 4G). The results of Western blotting corroborated the RT-qPCR findings (Figure 4H), and all of the observed indicators were strong profibrotic factors, as previously mentioned. Taken together, these results show that rapamycin application significantly reduces skin damage and fibrotic changes, indicating that autophagy plays a protective role after radiation exposure.

3.5 | Modulation of Akt–mTOR pathway following topical rapamycin application

To elucidate the mechanism underlying the mitigating effects of rapamycin on radiation dermatitis, we investigated the Akt–mTOR pathway, a well-known signaling pathway related to a major regulator and an upstream signaling pathway of autophagy.[36] First, we examined the autophagy activity among the three groups, all of which received a single fraction of 30 Gy with 6-MeV electrons (Figure 5A). Quantitative analysis of the immunofluorescence intensity of LC3B in the skin tissue of the three groups revealed the weakest cytoplasmic staining

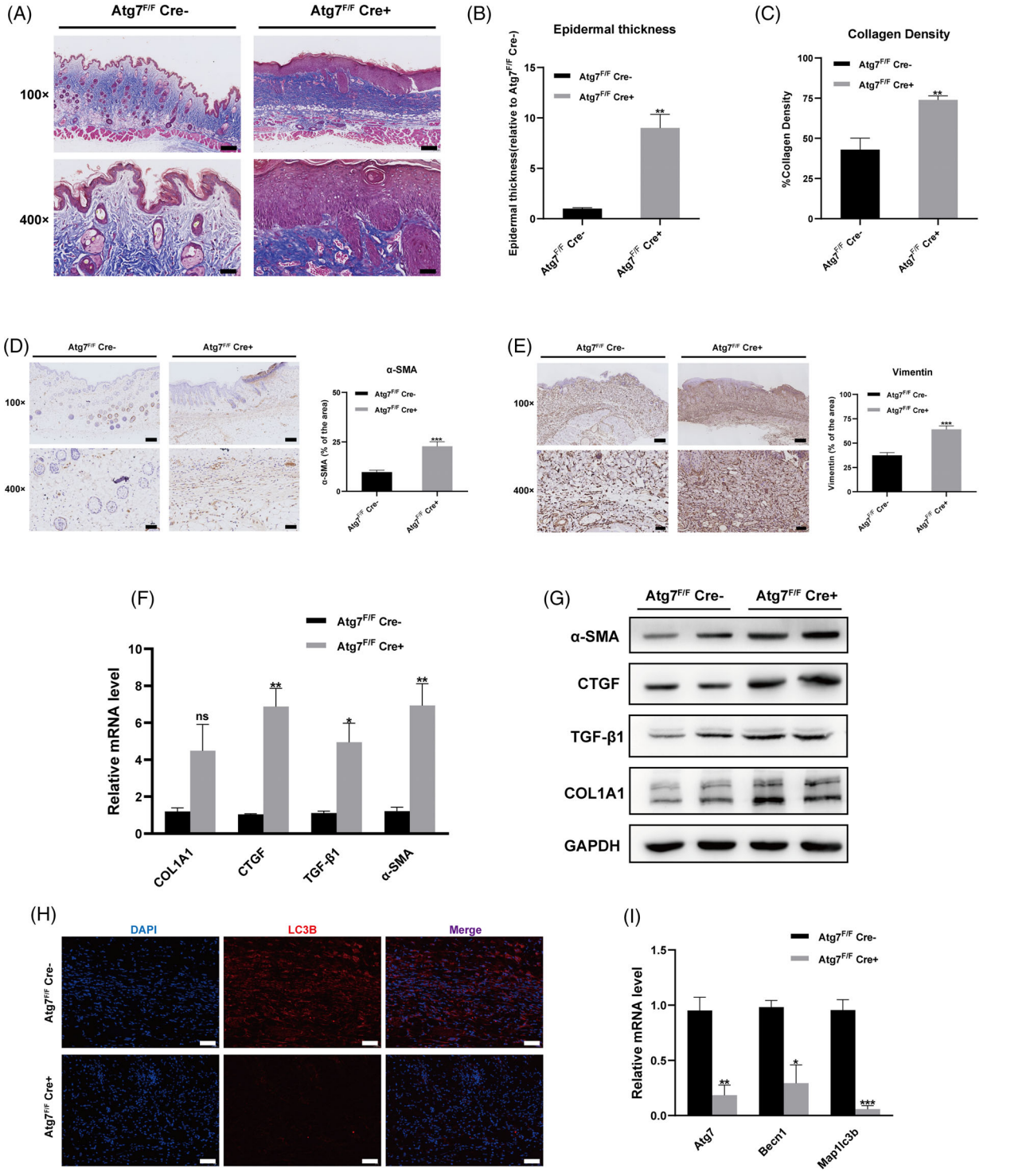

FIGURE 3 Deletion of Atg7 is related to the histological, gene and protein expression level changes in the skin tissues after irradiation. (A) Representative images of Masson's trichrome staining of $Atg7^{Flox/Flox}$ Cre^{+} and $Atg7^{Flox/Flox}$ Cre^{-} mice skin tissue 30 days post irradiation, with collagen fibers dyed blue. Magnification 100× and 400×, scale bar 200 and 50 μm, respectively. (B) Epidermal thickness (red stained in A). (C) Collagen density (blue stained in A) was quantified using the ImageJ software. (D and E) Representative IHC sections of α-SMA and vimentin in the $Atg7^{Flox/Flox}$ Cre^{+} and $Atg7^{Flox/Flox}$ Cre^{-} mice skin tissue 30 days post irradiation. The bar graphs on the right show the results of quantitative analyses. Magnification 100× and 400×, scale bar 200 and 50 μm, respectively. (F) Total skin lysates of two different groups ($Atg7^{Flox/Flox}$ Cre^{+} and $Atg7^{Flox/Flox}$ Cre^{-}) at 30 days post irradiation were subjected to Western blot analysis for COL1A1, CTGF, TGF-β1, and α-SMA, and one representative experiment from three independent experiments is shown. (G) qPCR analysis of COL1A1, CTGF, TGF-β1, and α-SMA in mouse skin. (H) Immuno-fluorescent staining for LC3B of mice skin tissue at 30 days after irradiation. Magnification 400×; scale bar 50 μm. (I) qPCR analysis of Atg7, Becn1, and Map1lc3b in the mouse skin tissue. Data are presented as means ± SEM; $n = 6$ mice per group. *Student's t-test $p < 0.05$, **Student's t-test $p < 0.01$, ***Student's t-test $p < 0.001$. ns: non-significant, Student's t-test.

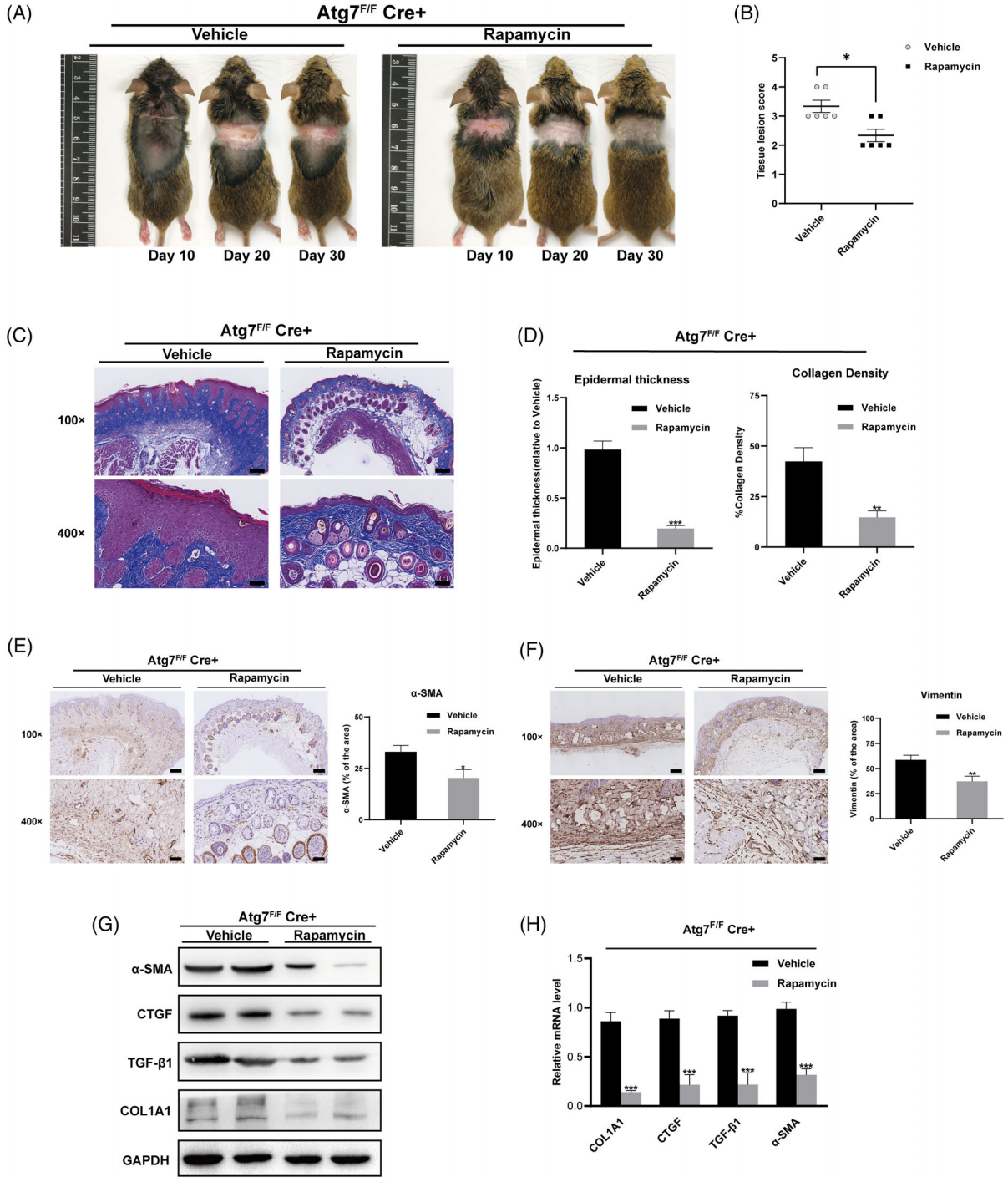

FIGURE 4 Efficacy of topical rapamycin application against radiation-induced skin injury and it reduces dermal fibrosis. (A) Representative photographs of the dorsal skin of the two different groups treated with vehicle or rapamycin at different time points after irradiation. (B) RTOG score of radiation-induced dermatitis in the dorsal skin of two different groups of mice. Statistical significance was estimated using the Mann–Whitney *U* test, * $p < 0.05$, $Z = -2.447$. (C) Representative images of Masson's trichrome-stained two different groups treated with vehicle or rapamycin skin tissue at 30 days post irradiation, with collagen fibers dyed blue. Magnification 100× and 400×; scale bar: 200 and 50 μm, respectively. (D) Epidermal thickness (red stained in C), and collagen density (blue stained in C) are quantified using the ImageJ software. (E and F) Representative IHC sections of α-SMA and vimentin in the two different groups treated with vehicle or rapamycin skin tissue at 30 days post irradiation. The bar graphs on the right show the results of quantitative analyses. Magnification 100× and 400×; scale bar: 200 and 50 μm, respectively. (G) Total skin lysates of two different groups (treated with vehicle or rapamycin) at 30 days post irradiation are subjected to Western blot analysis for COL1A1, CTGF, TGF-β1, and α-SMA, and one representative experiment from three independent experiments is shown. (H) Quantitative real-time PCR analysis of COL1A1, CTGF, TGF-β1, and α-SMA in the mouse skin. Total RNAs are extracted from the skin of two different groups treated with vehicle or rapamycin. Data are presented as means ± SEM; $n = 6$ mice per group. *Student's *t*-test $p < 0.05$, **Student's *t*-test $p < 0.01$, ***Student's *t*-test $p < 0.001$.

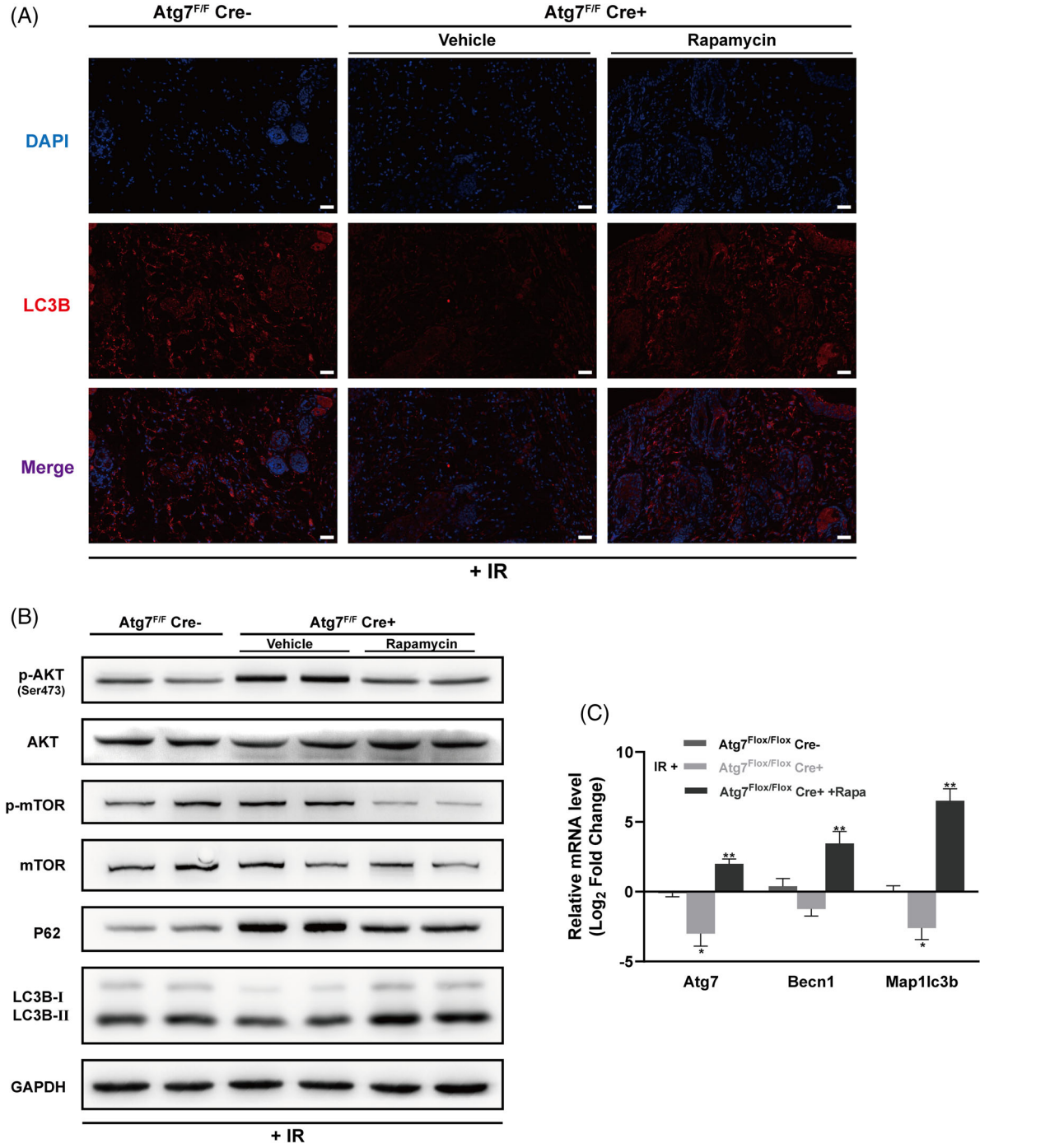

FIGURE 5 Modulation of Akt–mTOR pathway following topical rapamycin application. (A) Immunofluorescence staining for LC3B in the skin tissue of the three groups 30 days after irradiation. Magnification 400×; scale bar: 20 μm. (B) Western blot of p-AKT Ser473, AKT, p-mTOR, mTOR, P62, and LC3B-II/LC3B-I in the skin tissue of the three groups at 30 days after irradiation. (C) qPCR analysis of Atg7, Becn1, and Map1lc3b in the skin tissue of the three groups 30 days after irradiation. IR, irradiation. Data are presented as means ± SEM. *Student's *t*-test $p < 0.05$, **Student's *t*-test $p < 0.01$.

intensity of LC3B occurring in $Atg7^{Flox/Flox}$ Cre^{+} with vehicle group, whereas the immunofluorescence intensity was higher in $Atg7^{Flox/Flox}$ Cre^{+} with rapamycin compared to the vehicle group (Figure 5A). These results clearly suggested a defect in autophagy after Atg7 conditional knockout, as well as a reactivation of autophagy after rapamycin treatment. Western blot results also provided supporting evidence for the autophagy status by showing the significant changes in the expression of LC3B-II/GAPDH ratio and p62 after rapamycin treatment (Figure 5B). Furthermore, treatment with topical rapamycin significantly decreased the expressions of p-Akt Ser473 and p-mTOR

in skin lysates extracted from the three groups (Figure 5B). The autophagy-related indicators detected by qPCR analyses further confirmed that the autophagy flux impaired by Atg7 conditional knockout was rescued by rapamycin (Figure 5C). Altogether, these results show that rapamycin significantly induces autophagy via inactivation of Akt–mTOR signaling pathway.

3.6 | Induction of autophagy by rapamycin alleviates fibrogenesis induced by radiation in vitro

To confirm the role of autophagy in vitro, we used ATG7-siRNA to knockdown ATG7 expression in vitro. Human foreskin fibroblast (HFF-1) cells were transfected with si-NC or three ATG7 siRNAs for 48 h and then analyzed by qPCR and Western blotting to determine transfection efficiency. Given that si-ATG7-1 had the highest knockdown efficiency, it was selected for further experiments (Figure 6A,B). To verify whether the autophagy effects in vitro were the same as those in vivo after irradiation, we irradiated HFF-1 cells transfected with si-NC or si-ATG7 for 48 h with a single dose of 8 Gy, and the rapamycin group was treated with 100 nM rapamycin for 24 h. We found an upregulation of the protein levels of fibrosis markers such as COL1A and α-SMA in si-ATG7-transfected cells compared with cells transfected with si-NC, whereas the rapamycin group exhibited marked decreases in these indicators (Figure 6C). In particular, the alleviation of fibrosis by rapamycin treatment was significantly blunted when 3-MA inhibited autophagy (Figure 6C). Some fibrosis markers showed no statistical significance for this trend and are not shown in the figure. We also found that upregulation of the mRNA levels of fibrosis markers, such as COL1A and α-SMA in si-ATG7-transfected cells compared with cells transfected with si-NC and rapamycin attenuated the upregulation of indicators of fibrosis (Figure 6D). Consistent with the Western blotting results, autophagy blockage by 3-MA abolished the alleviation of fibrosis caused by rapamycin treatment (Figure 6D). Altogether, these results indicate that fibrogenesis in si-ATG7 HFF-1 cells after irradiation is reversed by rapamycin, but inhibition of autophagy by 3-MA abolishes this effect.

To further determine whether the Akt–mTOR pathway is involved, we analyzed the key protein levels of this autophagy-related pathway. Variation trends of p-Akt Ser473, p-mTOR, and other indicators of autophagy agreed with the trends observed in the in vivo experiments (Figure 6E). Furthermore, autophagy status was also defined using immunofluorescence microscopy of HFF-1 cells transfected with mCherry-GFP-LC3B tandem reporter adenovirus.[37] Our immunofluorescence results indicated that the HFF-1 cells with ATG7 knockdown contained fewer red-only puncta and yellow puncta compared to the si-NC group. In parallel, a significant elevation of both autophagosomes (yellow puncta) and autolysosomes (red puncta) was observed following rapamycin treatment. Additionally, in HFF-1 cells pretreated with 3-MA, we found that rapamycin was unable to induce adequate formation of yellow or red puncta in the rapamycin-treated group, confirming the inhibition of autophagy (Figure 6F).

3.7 | Impaired autophagy is associated with persistent activation of Nrf2

To further analyze the related molecules of the Atg7 protein, the online GeneMANIA tool (http://www.genemania.org/) was used.[38] Of great interest, the results showed that Atg7 directly interacts with Nrf2 (Nfe2l2) and Keap1 (Figure 7A). Meanwhile, interaction network analysis based on STRING (https://cn.string-db.org/) further confirmed the conclusions obtained by GeneMANIA (Figure 7B). Previous studies have suggested that defects in autophagy can cause sustained activation of Nrf2 by activating the non-canonical p62–Keap1–Nrf2 pathway.[39,40] The activation status of Nrf2-autophagy-related pathway was verified by qPCR of Nrf2 and its downstream gene expression under both in vivo and in vitro conditions. As described in Figure 7C–F, consistent with previous findings, qPCR analysis and Western blotting showed the aberrant upregulation of Nrf2 and its downstream gene (Nqo1 and Ho-1) in the impaired autophagy group, whereas rapamycin significantly reversed this phenomenon. However, as expected, pretreatment with 3-MA abolished the effect of rapamycin on the Nrf2-autophagy-related pathway. Collectively, these findings revealed that reactivation of autophagy could downregulate the abnormal activation of the Nrf2-related pathway, indicating that persistent activation of Nrf2 might contribute to radiation-induced fibrogenesis associated with Atg7 deficiency.

4 | DISCUSSION

In the present study, we characterized the pathological and morphological changes occurring in the skin of Atg7 mice with myofibroblast-specific deletion after irradiation. Our results showed that impaired autophagy due to Atg7 deletion increased the severity of skin damage associated with radiation exposure, especially the severity of skin fibrotic changes. More importantly, we demonstrated that the activation of the Akt–mTOR pathway contributed to the pathogenesis of this process. We also found that rapamycin alleviated radiation-induced injury by reactivating autophagy. Our findings provide compelling evidence that deletion of myofibroblast autophagy gene Atg7 leads to more severe radiation-induced cutaneous injury and further fibrosis in response to electron beam radiation. Altogether, these data suggest that the autophagy gene Atg7 is a protective factor against radiation-induced skin injury in both in vivo murine genetic models and in vitro cellular studies.

Radiation-induced skin damage is an inevitable complication of radiation therapy. Nevertheless, no standard criteria currently exist for the treatment of radiation-induced skin injuries.[41] An essential aspect of our study was to determine whether autophagy induction can be used as a therapeutic intervention for radiation-induced skin injury. Autophagy is a conserved catabolic process that removes damaged organelles or proteins via the lysosomal degradation pathway.[9] Autophagy dysfunction has been shown to be associated with several pathologies and diseases, including cancer, neurodegenerative

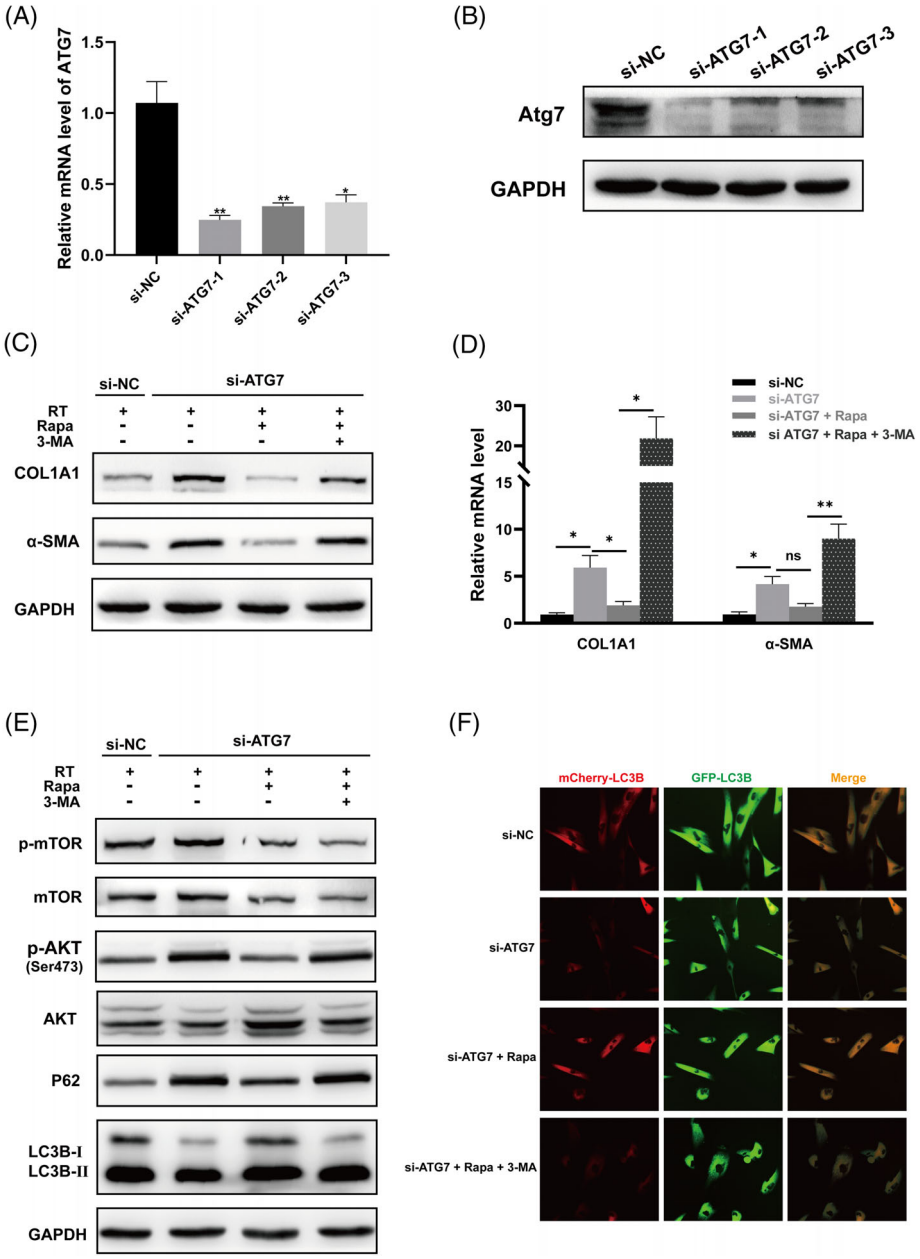

FIGURE 6 Induction of autophagy by rapamycin alleviates fibrogenesis induced by radiation in vitro. (A) qPCR analysis of the knockdown efficiency of ATG7 after 48 h siRNA transfection. (B) Western blot analysis of the knockdown efficiency of ATG7 after 48 h siRNA transfection. (C) Western blot of COL1A1 and α-SMA of si-NC, si-ATG7, si-ATG7 + Rapa, and si-ATG7 + Rapa + 3-MA groups of HFF-1 cells. (D) Quantitative real-time PCR analysis of COL1A1 and α-SMA of si-NC, si-ATG7, si-ATG7 + Rapa, and si-ATG7 + Rapa + 3-MA groups of HFF-1 cells. (E) Western blot of p-AKT Ser473, AKT, p-mTOR, mTOR, P62, and LC3B-II/LC3B-I in si-NC, si-ATG7, si-ATG7 + Rapa, and si-ATG7+ Rapa + 3-MA groups of HFF-1 cells. (F) Autophagy status is evaluated by mCherry-GFP-LC3B puncta formation in si-NC, si-ATG7, si-ATG7 + Rapa, and si-ATG7 + Rapa + 3-MA groups of HFF-1 cells transfected with Ad-mCherry-GFP-LC3B, and images are captured using a fluorescent microscope. All HFF-1 cells received a single dose of 8 Gy irradiation. Representative Western blot images out of three independent experiments are shown. Rapa, rapamycin; 3-MA, 3-methyladenine; IR, irradiation. Data are presented as means ± SEM. *Student's *t*-test $p < 0.05$, **Student's *t*-test $p < 0.01$. ns: non-significant, Student's *t*-test.

diseases, infectious diseases, and autoimmune disorders.[10,42] Yi et al. demonstrated podocyte-specific Atg7 conditional knockout results in a more serious adriamycin-induced nephropathy.[43] Lee et al. confirmed that autophagy deficiency in myeloid-derived cell enhances susceptibility to experimental colitis and obesity-induced diabetes.[44] A recent study reported that keratinocyte autophagy deficiency inhibits cutaneous wound healing.[12] Autophagy activation has also been shown to protect keratinocyte against inflammatory responses and UVB-induced skin photodamage.[45,46] HMGB1/RAGE promotes autophagy, thereby protecting keratinocytes from UV radiation-induced cell death, according to Mou et al.[47] Inhibition of mTOR leads to increased cytoprotective autophagy, which may contribute to the reduction in

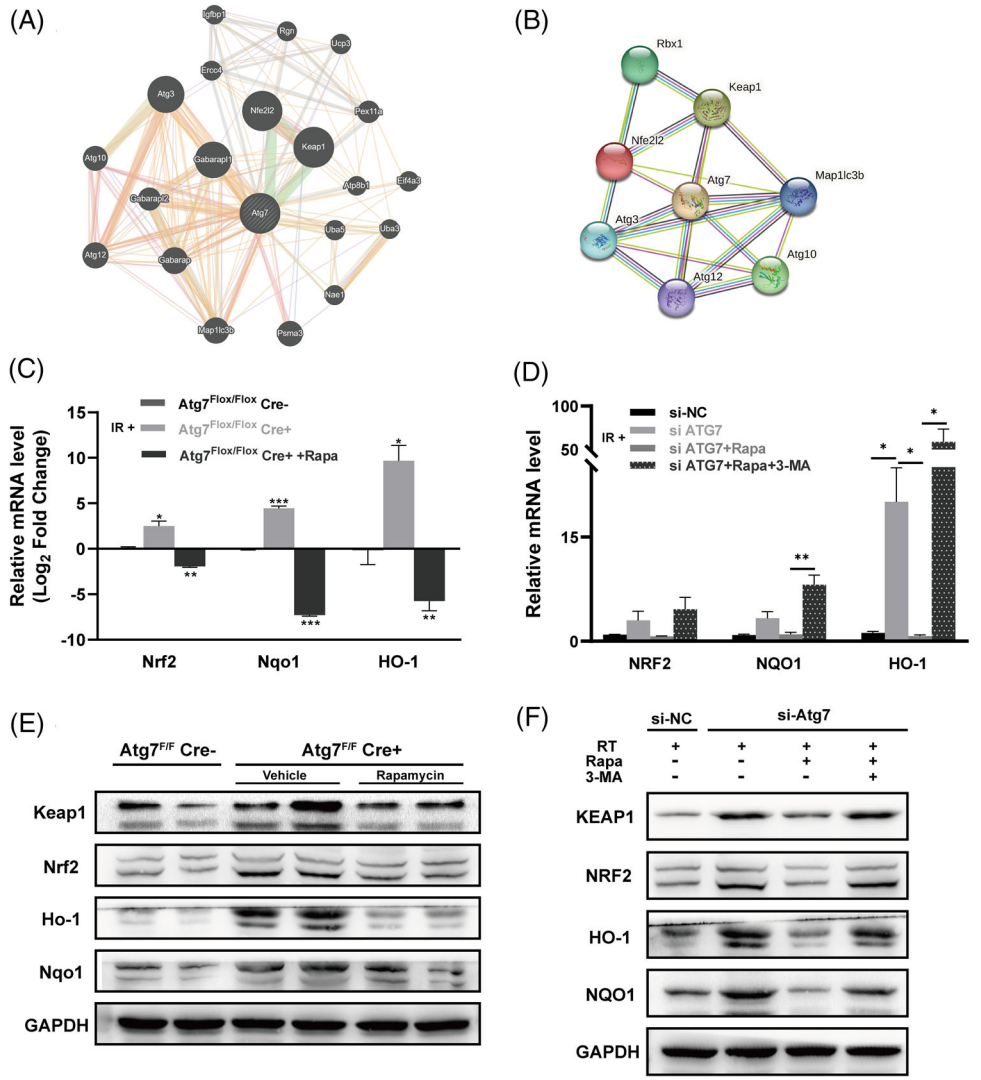

FIGURE 7 The impaired autophagy is associated with persistent activation of Nrf2 in vitro. (A and B) GeneMANIA (A) and STRING (B) protein–protein association networks of Atg7 gene. (C) Quantitative real-time PCR analysis of Nrf2, Nqo1, and Ho-1 in the mouse skin among the three groups. (D) Quantitative real-time PCR analysis of NRF2, NQO1, and HO-1 in si-NC, si-ATG7, si-ATG7 + Rapa, and si-ATG7 + Rapa + 3-MA groups of HFF-1 cells after a single dose of 8 Gy irradiation. (E) Western blot of Keap1, Nrf2, Ho-1, and Nqo1 in mouse skin among the three groups. (F) Western blot of KEAP1, NRF2, HO-1, and NQO1 in si-NC, si-si-ATG7, si-ATG7 + Rapa, and si-ATG7 + Rapa + 3-MA groups of HFF-1 cells after a single dose of 8 Gy irradiation. Data are presented as means ± SEM. *Student's *t*-test $p < 0.05$, **Student's *t*-test $p < 0.01$, ***Student's *t*-test $p < 0.001$.

the UVB-induced abnormal proliferation of keratinocytes and have important implications for skin cancer prevention.[47] Hao et al. demonstrated that Sanshool protects human dermal fibroblasts against UVB-induced damage by activating autophagy.[13] Therefore, we were interested to know whether autophagy-related mechanisms were involved in radiation-induced skin damage.

Radiation-induced fibrosis is known to occur in various tissues and organs.[7] Several studies have also indicated an association between autophagy and fibrosis. Moreover, chronic liver injury and liver fibrosis are associated with impaired autophagy,[48–50] and that triggering autophagy diminishes the expression of COL1A1 in HSCs.[51] A recent study published by Seo et al. in the last few months has further confirmed that the autophagy defect caused by the lack of Atg7 in the liver leads to the occurrence of liver fibrosis.[52] Researchers have also emphasized the protective role of autophagy during fibrosis of various tissues, such as the kidney[53] and heart.[54] More importantly, autophagy is essential for wound healing,[22] and autophagy deficiency can lead to abnormal wound repair with excessive ECM deposition. For instance, collagen deposition has been shown to significantly increase when autophagy is impaired during tendon injury repair.[32] Autophagy is also closely related to the homeostasis of tissue architecture and function.[55] Shi et al. demonstrated that IL10 could inhibit autophagy through signaling via both the IL10/IL10R-STAT3 and IL10/Akt–mTOR pathways, which have potential therapeutic benefits in the prevention and reduction of a severe skin fibrotic disease called hypertrophic scar (HS).[56] Another study conducted by Shi et al., which attempted

to probe into the underlying mechanisms of autophagy in HS formation, indicated that autophagy protein LC3 regulates the fibrosis of HS by controlling Bcl-xL in dermal fibroblasts.[57] Furthermore, Pang et al. demonstrated that resveratrol inhibits HS viability by activating autophagy via the miR-4654/Rheb axis.[58] Based on the above studies, whether autophagy activity has an effect on radiation-induced skin damage by infecting fibrotic changes warrants our further investigation.

We applied myofibroblast-specific conditional Atg7 knockout mice in our study. As we know, Atg7 is a core autophagic-machinery component due to its role in ubiquitin-like reactions.[59] Meanwhile, it has been widely acknowledged that myofibroblasts play essential roles in the fibrogenesis process and cause ECM protein accumulation, specifically after tissues injury.[7,60] Thus, this animal model can confirm whether the abnormal skin fibrogenesis process upon Atg7 deletion is autophagy dependent. With the impaired autophagy caused by Atg7 deletion, it is possible that some newly synthesized proteins during skin wound healing post irradiation are not cleared efficiently, and that accumulation of these proteins may cause proteotoxicity, resulting in myofibroblast malfunction and a more severe phenotype in irradiated skin.

To further clarify the possible role of autophagy in radiation-induced skin injury and fibrotic changes, $Atg7^{Flox/Flox}$ Pdgfrb-Cre^{+} mice were treated with rapamycin to rescue autophagy. As principal methods for assessment of autophagy activity, the content of LC3-II protein, which is converted from LC3-I, is widely used as a standard indicator to monitor the number of autophagosomes.[61] In addition to LC3-II, p62 can also be used as an indicator of autophagy activity, and p62 accumulates when autophagy is deficient but decreases when autophagy is activated.[31,62] However, in addition to the canonical autophagic pathway, there is evidence suggesting the presence of several non-canonical autophagy pathways, which is Atg7-independent alternative autophagy and is regulated by Ulk1 and beclin 1.[63] Although the conversion from LC3-I to LC3-II is generally considered a good indicator of autophagy, it does not occur during the Atg7-independent alternative process of autophagy.[64] Therefore, the detection for this indicator provides evidence supporting the occurrence of Atg7-dependent autophagy. As previously stated, our results confirmed that rapamycin successfully reactivated autophagy based on the increased expression of LC3-II and decreased expression of p62 (Figure 5). TGF-β1 is one of the most essential profibrotic factors, which strongly enhances fibroblast proliferation and stimulates ECM synthesis. CTGF binds directly to TGF-β1 to exert a synergistic effect on fibrogenesis and regulate TGF-β1 expression in a positive feedback loop manner.[65] As expected, our results demonstrated that rapamycin significantly decreased the generation of TGF-β1 and CTGF after irradiation, thereby decreasing the synthesis of COL1A1 and fibronectin. These changes were under the premise that rapamycin successfully reactivates autophagy. Additionally, we found that rapamycin induced protective autophagy by inhibiting the Akt–mTOR signaling pathway (Figure 5B), which suppresses autophagy when it is activated in mammalian cells and promotes autophagy when it is inactivated.[66] However, pretreatment with 3-MA, which blocks autophagosome formation by inhibiting class III PI3K,[67] abolishes all the effects caused by autophagy reactivation. In addition, Nrf2 is known as a dominant regulator of cellular redox homeostasis.[68] The role of Nrf2 in radiation (ionizing, ultraviolet)-induced carcinogenesis has also been clearly established, with decades of studies on chemoprevention and cellular defense using $Nrf2^{-/-}$ mice.[69,70] In contrast, the association between Nrf2 signaling and autophagy appeared to be strong. Autophagic degradation of Keap1 through its interaction with p62, which competes with Nrf2 to bind to Keap1, contributes to maintaining redox homeostasis.[71] As already concluded by Ni et al., Nrf2 contributes to the development of fibrosis in mice with defective hepatic autophagy.[49] Thus, we measured the expression of Nrf2 and Nrf2-downstream antioxidant genes Nqo1 and HO-1. The results demonstrated that the Nrf2-related pathway was activated in the groups with impaired autophagy. These striking differences provided some insights and speculations regarding the relationships between persistent activation of Nrf2 and radiation-induced fibrogenesis associated with Atg7 deficiency. In summary, our findings indicate that rapamycin may serve as an efficient therapeutic strategy to prevent skin damage, particularly fibrosis after irradiation, and that the molecular mechanism might be closely related to the Akt–mTOR and Nrf2-autophagy-related pathways.

However, this study has several limitations that need to be addressed. First, fractionated radiotherapy is more common clinically than single high-dose radiotherapy. Moreover, fractionated radiotherapy commonly causes more severe radiation-induced skin damage than a single high-dose radiotherapy, because the continuous impact of irradiation disturbs skin self-renewal. However, owing to the limitations of the experimental conditions, the present models did not adequately simulate clinical situations. Also due to the limitation of experimental conditions, while it may be tempting for us to perform transmission electron microscopy (TEM), which is considered the gold standard to assess autophagy, we were not able to conduct these experiments. In addition, the mechanisms underlying the effects of rapamycin were not sufficiently explored. Hence, the exact molecular mechanism and regulation of the impact of rapamycin on the Akt–mTOR pathway and its downstream targets warrant further elaborate investigation. We hope that these limitations will be refined in future studies.

5 | CONCLUSIONS

Our data show that topical rapamycin-treated mice are protected against radiation-induced cutaneous injury and further fibrosis in myofibroblast-specific deletion of Atg7, with decreased epidermal thickness and dermal collagen deposition, as well as improved wound healing in irradiated skin compared with the vehicle group mice. Therefore, targeting the autophagy-related pathway may be useful for preventing or ameliorating radiation changes in the skin, which can be a novel therapeutic strategy in clinical practice.

ACKNOWLEDGMENTS

The authors sincerely thank all the participants involved in this study.

CONFLICT OF INTEREST STATEMENT

The authors declare that they have no conflicts of interest.

DATA AVAILABILITY STATEMENT

The data used to support the findings of this study are available from the corresponding author upon request.

ETHICS STATEMENT

Ethical approval for this study (Ethical Committee TJH-201906013) was provided on June 2019 by the Tongji Hospital Institutional Review Board of Experimental Animals.

ORCID

Xinyi Chen https://orcid.org/0000-0002-0638-1380

REFERENCES

1. Thomas GM. Is there a role for consolidation or salvage radiotherapy after chemotherapy in advanced epithelial ovarian cancer? *Gynecol Oncol*. 1993;51(1):97-103. https://doi.org/10.1006/gyno.1993.1253
2. Chan RJ, Webster J, Chung B, et al. Prevention and treatment of acute radiation-induced skin reactions: a systematic review and meta-analysis of randomized controlled trials. *BMC Cancer*. 2014;14:53. https://doi.org/10.1186/1471-2407-14-53
3. Ryan JL. Ionizing radiation: the good, the bad, and the ugly. *J Invest Dermatol*. 2012;132(3 Pt 2):985-993. https://doi.org/10.1038/jid.2011.411
4. Singh M, Alavi A, Wong R, et al. Radiodermatitis: a review of our current understanding. *Am J Clin Dermatol*. 2016;17(3):277-292. https://doi.org/10.1007/s40257-016-0186-4
5. Chen YP, Tsang NM, Tseng CK, et al. Causes of interruption of radiotherapy in nasopharyngeal carcinoma patients in Taiwan. *Jpn J Clin Oncol*. 2000;30(5):230-234. https://doi.org/10.1093/jjco/hyd059
6. Kim JH, Kolozsvary AJ, Jenrow KA, et al. Mechanisms of radiation-induced skin injury and implications for future clinical trials. *Int J Radiat Biol*. 2013;89(5):311-318. https://doi.org/10.3109/09553002.2013.765055
7. Ejaz A, Greenberger JS, Rubin PJ. Understanding the mechanism of radiation induced fibrosis and therapy options. *Pharmacol Ther*. 2019;204:107399. https://doi.org/10.1016/j.pharmthera.2019.107399
8. Bolderston A, Lloyd NS, Wong RK, et al. The prevention and management of acute skin reactions related to radiation therapy: a systematic review and practice guideline. *Support Care Cancer*. 2006;14(8):802-817. https://doi.org/10.1007/s00520-006-0063-4
9. Mizushima N. Autophagy: process and function. *Genes Dev*. 2007;21(22):2861-2873. https://doi.org/10.1101/gad.1599207
10. Levine B, Kroemer G. Autophagy in the pathogenesis of disease. *Cell*. 2008;132(1):27-42. https://doi.org/10.1016/j.cell.2007.12.018
11. Qiang L, Sample A, Shea CR, et al. Autophagy gene ATG7 regulates ultraviolet radiation-induced inflammation and skin tumorigenesis. *Autophagy*. 2017;13(12):2086-2103. https://doi.org/10.1080/15548627.2017.1380757
12. Qiang L, Yang S, Cui YH, et al. Keratinocyte autophagy enables the activation of keratinocytes and fibroblasts and facilitates wound healing. *Autophagy*. 2020:2128-2143. https://doi.org/10.1080/15548627.2020.1816342
13. Hao D, Wen X, Liu L, et al. Sanshool improves UVB-induced skin photodamage by targeting JAK2/STAT3-dependent autophagy. *Cell Death Dis*. 2019;10(1):19. https://doi.org/10.1038/s41419-018-1261-y
14. Huang S, Huang Y, Lin W, et al. Sitagliptin alleviates radiation-induced intestinal injury by activating NRF2-antioxidant axis, mitigating NLRP3 inflammasome activation, and reversing gut microbiota disorder. *Oxid Med Cell Longev*. 2022;2022:2586305. https://doi.org/10.1155/2022/2586305
15. Nie X, Yu Q, Li L, et al. Kinsenoside protects against radiation-induced liver fibrosis via downregulating connective tissue growth factor through TGF-beta1 signaling. *Front Pharmacol*. 2022;13:808576. https://doi.org/10.3389/fphar.2022.808576
16. Li L, Nie X, Yi M, et al. Aerosolized thyroid hormone prevents radiation induced lung fibrosis. *Front Oncol*. 2020;10:528686. https://doi.org/10.3389/fonc.2020.528686
17. Luo XX, Yang C, Zhan GF, et al. Whole brain radiotherapy induces cognitive dysfunction in mice: key role of gut microbiota. *Psychopharmacology (Berl)*. 2020;237(7):2089-2101. https://doi.org/10.1007/s00213-020-05520-0
18. Li L, Nie X, Zhang P, et al. Dexrazoxane ameliorates radiation-induced heart disease in a rat model. *Aging (Albany NY)*. 2021;13(3):3699-3711. doi: 10.18632/aging.202332
19. Komatsu M, Waguri S, Ueno T, et al. Impairment of starvation-induced and constitutive autophagy in Atg7-deficient mice. *J Cell Biol*. 2005;169(3):425-434. https://doi.org/10.1083/jcb.200412022
20. Phan SH. The myofibroblast in pulmonary fibrosis. *Chest*. 2002;122(6 Suppl):286S-289S. https://doi.org/10.1378/chest.122.6_suppl.286s
21. Evdokiou A, Kanisicak O, Gierek S, et al. Characterization of burn eschar pericytes. *J Clin Med*. 2020;9(2):606. https://doi.org/10.3390/jcm9020606
22. Li H, Li D, Ma Z, et al. Defective autophagy in osteoblasts induces endoplasmic reticulum stress and causes remarkable bone loss. *Autophagy*. 2018;14(10):1726-1741. https://doi.org/10.1080/15548627.2018.1483807
23. Cuttler AS, LeClair RJ, Stohn JP, et al. Characterization of Pdgfrb-Cre transgenic mice reveals reduction of ROSA26 reporter activity in remodeling arteries. *Genesis*. 2011;49(8):673-680. https://doi.org/10.1002/dvg.20769
24. Cao J, Ding K, Pan G, et al. Deletion of PPARgamma in mesenchymal lineage cells protects against aging-induced cortical bone loss in mice. *J Gerontol A Biol Sci Med Sci*. 2020;75(5):826-834. https://doi.org/10.1093/gerona/glaa049
25. Liu F, Woitge HW, Braut A, et al. Expression and activity of osteoblast-targeted Cre recombinase transgenes in murine skeletal tissues. *Int J Dev Biol*. 2004;48(7):645-653. https://doi.org/10.1387/ijdb.041816fl
26. Arifin WN, Zahiruddin WM. Sample size calculation in animal studies using resource equation approach. *Malays J Med Sci*. 2017;24(5):101-105. https://doi.org/10.21315/mjms2017.24.5.11
27. Yang F, Tanaka M, Wataya-Kaneda M, et al. Topical application of rapamycin ointment ameliorates *Dermatophagoides farinae* body extract-induced atopic dermatitis in NC/Nga mice. *Exp Dermatol*. 2014;23(8):568-572. https://doi.org/10.1111/exd.12463
28. Reisman SA, Lee CY, Meyer CJ, et al. Topical application of the synthetic triterpenoid RTA 408 protects mice from radiation-induced dermatitis. *Radiat Res*. 2014;181(5):512-520. https://doi.org/10.1667/RR13578.1
29. Ning S, Budas GR, Churchill EN, et al. Mitigation of radiation-induced dermatitis by activation of aldehyde dehydrogenase 2 using topical alda-1 in mice. *Radiat Res*. 2012;178(1):69-74. https://doi.org/10.1667/rr2861.1
30. Cao J, Zhu W, Yu D, et al. The involvement of SDF-1alpha/CXCR4 axis in radiation-induced acute injury and fibrosis of skin. *Radiat Res*. 2019;192(4):410-421. https://doi.org/10.1667/RR15384.1
31. Komatsu M, Ichimura Y. Physiological significance of selective degradation of p62 by autophagy. *FEBS Lett*. 2010;584(7):1374-1378. https://doi.org/10.1016/j.febslet.2010.02.017
32. Zheng W, Qian Y, Chen S, et al. Rapamycin protects against peritendinous fibrosis through activation of autophagy. *Front Pharmacol*. 2018;9:402. https://doi.org/10.3389/fphar.2018.00402

33. Yoshizaki A, Yanaba K, Yoshizaki A, et al. Treatment with rapamycin prevents fibrosis in tight-skin and bleomycin-induced mouse models of systemic sclerosis. *Arthritis Rheum*. 2010;62(8):2476-2487. https://doi.org/10.1002/art.27498
34. Greveling K, Prens EP, van Doorn MB. Treatment of port wine stains using pulsed dye laser, erbium YAG laser, and topical rapamycin (sirolimus) – a randomized controlled trial. *Lasers Surg Med*. 2017;49(1):104-109. https://doi.org/10.1002/lsm.22548
35. Bridle KR, Popa C, Morgan ML, et al. Rapamycin inhibits hepatic fibrosis in rats by attenuating multiple profibrogenic pathways. *Liver Transpl*. 2009;15(10):1315-1324. https://doi.org/10.1002/lt.21804
36. Heras-Sandoval D, Perez-Rojas JM, Hernandez-Damian J, et al. The role of PI3K/AKT/mTOR pathway in the modulation of autophagy and the clearance of protein aggregates in neurodegeneration. *Cell Signal*. 2014;26(12):2694-2701. https://doi.org/10.1016/j.cellsig.2014.08.019
37. Pankiv S, Clausen TH, Lamark T, et al. p62/SQSTM1 binds directly to Atg8/LC3 to facilitate degradation of ubiquitinated protein aggregates by autophagy. *J Biol Chem*. 2007;282(33):24131-24145. https://doi.org/10.1074/jbc.M702824200
38. Warde-Farley D, Donaldson SL, Comes O, et al. The GeneMANIA prediction server: biological network integration for gene prioritization and predicting gene function. *Nucleic Acids Res*. 2010;38(Web Server issue):W214-W220. https://doi.org/10.1093/nar/gkq537
39. Komatsu M, Kurokawa H, Waguri S, et al. The selective autophagy substrate p62 activates the stress responsive transcription factor Nrf2 through inactivation of Keap1. *Nat Cell Biol*. 2010;12(3):213-223. https://doi.org/10.1038/ncb2021
40. Tang Z, Hu B, Zang F, et al. Nrf2 drives oxidative stress-induced autophagy in nucleus pulposus cells via a Keap1/Nrf2/p62 feedback loop to protect intervertebral disc from degeneration. *Cell Death Dis*. 2019;10(7):510. https://doi.org/10.1038/s41419-019-1701-3
41. Rosenthal A, Israilevich R, Moy R. Management of acute radiation dermatitis: a review of the literature and proposal for treatment algorithm. *J Am Acad Dermatol*. 2019;81(2):558-567. https://doi.org/10.1016/j.jaad.2019.02.047
42. Mizushima N, Levine B. Autophagy in human diseases. *N Engl J Med*. 2020;383(16):1564-1576. https://doi.org/10.1056/NEJMra2022774
43. Yi M, Zhang L, Liu Y, et al. Autophagy is activated to protect against podocyte injury in adriamycin-induced nephropathy. *Am J Physiol Renal Physiol*. 2017;313(1):F74-F84. https://doi.org/10.1152/ajprenal.00114.2017
44. Lee HY, Kim J, Quan W, et al. Autophagy deficiency in myeloid cells increases susceptibility to obesity-induced diabetes and experimental colitis. *Autophagy*. 2016;12(8):1390-1403. https://doi.org/10.1080/15548627.2016.1184799
45. Lee HM, Shin DM, Yuk JM, et al. Autophagy negatively regulates keratinocyte inflammatory responses via scaffolding protein p62/SQSTM1. *J Immunol*. 2011;186(2):1248-1258. https://doi.org/10.4049/jimmunol.1001954
46. Li L, Chen HY, Chen X, et al. Trehalose protects keratinocytes against ultraviolet B radiation by activating autophagy via regulating TIMP3 and ATG9A. *Oxid Med Cell Longev*. 2022;2022:9366494.
47. Mou K, Liu W, Han D, et al. HMGB1/RAGE axis promotes autophagy and protects keratinocytes from ultraviolet radiation-induced cell death. *J Dermatol Sci*. 2017;85(3):162-169. https://doi.org/10.1016/j.jdermsci.2016.12.011
48. Bridgeman BB, Wang P, Ye B, et al. Inhibition of mTOR by apigenin in UVB-irradiated keratinocytes: a new implication of skin cancer prevention. *Cell Signal*. 2016;28(5):460-468. https://doi.org/10.1016/j.cellsig.2016.02.008
49. Ni HM, Chao X, Yang H, et al. Dual roles of mammalian target of rapamycin in regulating liver injury and tumorigenesis in autophagy-defective mouse liver. *Hepatology*. 2019;70(6):2142-2155. https://doi.org/10.1002/hep.30770
50. Ni HM, Woolbright BL, Williams J, et al. Nrf2 promotes the development of fibrosis and tumorigenesis in mice with defective hepatic autophagy. *J Hepatol*. 2014;61(3):617-625. https://doi.org/10.1016/j.jhep.2014.04.043
51. Hidvegi T, Ewing M, Hale P, et al. An autophagy-enhancing drug promotes degradation of mutant alpha1-antitrypsin Z and reduces hepatic fibrosis. *Science*. 2010;329(5988):229-232. https://doi.org/10.1126/science.1190354
52. Ge M, Liu H, Zhang Y, et al. The anti-hepatic fibrosis effects of dihydrotanshinone I are mediated by disrupting the yes-associated protein and transcriptional enhancer factor D2 complex and stimulating autophagy. *Br J Pharmacol*. 2017;174(10):1147-1160. https://doi.org/10.1111/bph.13766
53. Seo HY, Lee SH, Han E, et al. Increased levels of phosphorylated ERK induce CTGF expression in autophagy-deficient mouse hepatocytes. *Cells*. 2022;11(17):2704. https://doi.org/10.3390/cells11172704
54. Jia P, Cai H, Liu X, et al. Long non-coding RNA H19 regulates glioma angiogenesis and the biological behavior of glioma-associated endothelial cells by inhibiting microRNA-29a. *Cancer Lett*. 2016;381(2):359-369. https://doi.org/10.1016/j.canlet.2016.08.009
55. Liu S, Chen S, Li M, et al. Autophagy activation attenuates angiotensin II-induced cardiac fibrosis. *Arch Biochem Biophys*. 2016;590:37-47. https://doi.org/10.1016/j.abb.2015.11.001
56. Chang NC, Nguyen M, Bourdon J, et al. Bcl-2-associated autophagy regulator Naf-1 required for maintenance of skeletal muscle. *Hum Mol Genet*. 2012;21(10):2277-2287. https://doi.org/10.1093/hmg/dds048
57. Shi J, Wang H, Guan H, et al. IL10 inhibits starvation-induced autophagy in hypertrophic scar fibroblasts via cross talk between the IL10-IL10R-STAT3 and IL10-Akt–mTOR pathways. *Cell Death Dis*. 2016;7:e2133. https://doi.org/10.1038/cddis.2016.44
58. Shi J, Shi S, Wu B, et al. Autophagy protein LC3 regulates the fibrosis of hypertrophic scar by controlling Bcl-xL in dermal fibroblasts. *Oncotarget*. 2017;8(55):93757-93770.
59. Pang K, Li B, Tang Z, et al. Resveratrol inhibits hypertrophic scars formation by activating autophagy via the miR-4654/Rheb axis. *Mol Med Rep*. 2020;22(4):3440-52. https://doi.org/10.3892/mmr.2020.11407
60. Ohsumi Y. Molecular dissection of autophagy: two ubiquitin-like systems. *Nat Rev Mol Cell Biol*. 2001;2(3):211-216. https://doi.org/10.1038/35056522
61. Klingberg F, Hinz B, White ES. The myofibroblast matrix: implications for tissue repair and fibrosis. *J Pathol*. 2013;229(2):298-309. https://doi.org/10.1002/path.4104
62. Mizushima N, Yoshimori T, Levine B. Methods in mammalian autophagy research. *Cell*. 2010;140(3):313-326. https://doi.org/10.1016/j.cell.2010.01.028
63. Larsen KB, Lamark T, Overvatn A, et al. A reporter cell system to monitor autophagy based on p62/SQSTM1. *Autophagy*. 2010;6(6):784-793. https://doi.org/10.4161/auto.6.6.12510
64. Ra EA, Lee TA, Won Kim S, et al. TRIM31 promotes Atg5/Atg7-independent autophagy in intestinal cells. *Nat Commun*. 2016;7:11726. https://doi.org/10.1038/ncomms11726
65. Nishida Y, Arakawa S, Fujitani K, et al. Discovery of Atg5/Atg7-independent alternative macroautophagy. *Nature*. 2009;461(7264):654-658. https://doi.org/10.1038/nature08455
66. Abreu JG, Ketpura NI, Reversade B, et al. Connective-tissue growth factor (CTGF) modulates cell signalling by BMP and TGF-beta. *Nat Cell Biol*. 2002;4(8):599-604. https://doi.org/10.1038/ncb826
67. Alers S, Loffler AS, Wesselborg S, et al. Role of AMPK-mTOR-Ulk1/2 in the regulation of autophagy: cross talk, shortcuts, and feedbacks. *Mol Cell Biol*. 2012;32(1):2-11. https://doi.org/10.1128/MCB.06159-11
68. Klionsky DJ, Abeliovich H, Agostinis P, et al. Guidelines for the use and interpretation of assays for monitoring autophagy in higher eukaryotes. *Autophagy*. 2008;4(2):151-175. https://doi.org/10.4161/auto.5338

69. Ma Q. Role of nrf2 in oxidative stress and toxicity. *Annu Rev Pharmacol Toxicol*. 2013;53:401-426. https://doi.org/10.1146/annurev-pharmtox-011112-140320
70. Sekhar KR, Freeman ML. Nrf2 promotes survival following exposure to ionizing radiation. *Free Radic Biol Med*. 2015;88(Pt B):268-274. https://doi.org/10.1016/j.freeradbiomed.2015.04.035
71. Knatko EV, Ibbotson SH, Zhang Y, et al. Nrf2 activation protects against solar-simulated ultraviolet radiation in mice and humans. *Cancer Prev Res (Phila)*. 2015;8(6):475-486. https://doi.org/10.1158/1940-6207.CAPR-14-0362
72. Lau A, Zheng Y, Tao S, et al. Arsenic inhibits autophagic flux, activating the Nrf2-Keap1 pathway in a p62-dependent manner. *Mol Cell Biol*. 2013;33(12):2436-2446. https://doi.org/10.1128/MCB.01748-12
73. Cox JD, Stetz J, Pajak TF. Toxicity criteria of the Radiation Therapy Oncology Group (RTOG) and the European Organization for Research and Treatment of Cancer (EORTC). *Int J Radiat Oncol Biol Phys*. 1995;31(5):1341-1346. https://doi.org/10.1016/0360-3016(95)00060-C

SUPPORTING INFORMATION

Additional supporting information can be found online in the Supporting Information section at the end of this article.

How to cite this article: Chen X, Qin W, Wang L, Jin Y, Tu J, Yuan X. Autophagy gene Atg7 regulates the development of radiation-induced skin injury and fibrosis of skin. *Skin Res Technol*. 2023;29:e13337. https://doi.org/10.1111/srt.13337